

Shear viscosity of a hadron gas and influence of resonance lifetimes on relaxation time

J.-B. Rose^{1,2}, J. M. Torres-Rincon¹, A. Schäfer^{1,2}, D. R. Oliinychenko¹, and H. Petersen^{1,2,3}
¹*Frankfurt Institute for Advanced Studies, Ruth-Moufang-Strasse 1, 60438 Frankfurt am Main, Germany*
²*Institute for Theoretical Physics, Goethe University,
Max-von-Laue-Strasse 1, 60438 Frankfurt am Main, Germany and*
³*GSI Helmholtzzentrum für Schwerionenforschung, Planckstr. 1, 64291 Darmstadt, Germany*
(Dated: September 13, 2017)

We address a discrepancy between different computations of η/s (shear viscosity over entropy density) of hadronic matter. Substantial deviations of this coefficient are found between transport approaches mainly based on resonance propagation with finite lifetime and other (semi-analytical) approaches with energy-dependent cross-sections, where interactions do not introduce a timescale. We provide an independent extraction of this coefficient by using the newly-developed SMASH (Simulating Many Accelerated Strongly interacting Hadrons) transport code, which is an example of a mainly resonance-based approach. We compare the results from SMASH with numerical solutions of the Boltzmann equation for simple systems using the Chapman-Enskog expansion, as well as previous results in the literature. Our conclusion is that the hadron interaction via resonance formation/decay strongly affects the transport properties of the system, resulting in significant differences in η/s with respect to other approaches where binary collisions dominate. We argue that the relaxation time of the system—which characterizes the shear viscosity—is determined by the interplay between the mean-free time and the lifetime of resonances. We show how an artificial shortening of the resonance lifetimes, or the addition of a background elastic cross section nicely interpolate between the two discrepant results.

I. INTRODUCTION

Studying physical properties of hot and dense nuclear matter is one of the main goals of modern heavy-ion collision experiments. Among these properties, transport coefficients are key elements as they control the non-equilibrium evolution of the expanding fireball. One of the most well-studied dissipative coefficients is the shear viscosity η , which measures the ability of the fluid system to relax towards equilibrium after a shear perturbation [1, 2]. The interest in η substantially increased after the realization that (almost) ideal fluid dynamics was able to describe the high elliptic flow that has been measured at the Relativistic Heavy-Ion Collider [3, 4]. In 2003, the first analytical computation of the shear viscosity over entropy density in a strongly coupled conformal gauge theory using the anti-de Sitter/conformal field theory correspondence [5, 6] was performed. It was conjectured that $\eta/s = 1/(4\pi)$ represents a lower bound in any physical system, and in particular in Quantum Chromodynamics (QCD), the theory of strong interactions governing the evolution of a heavy ion collision. Extractions of the effective value of η/s by fitting relativistic viscous hydrodynamics to experimental measurements have been carried out since then [7, 8] (see [9] for an early estimate of η in the context of heavy ion collisions). These results showed that the average η/s in such systems is very close but slightly larger than the conjectured ratio. Some attempts to study the temperature dependence $\eta/s(T)$ from experimental data were also made within hydrodynamical [10, 11] and hybrid approaches [12, 13], and recent work has been done to extract it as part of a larger bayesian analysis of heavy ion collisions [14, 15]

The low temperature behavior of the shear viscosity

over entropy ratio can be constrained by calculations with hadronic degrees of freedom. For zero net baryon density, the shear viscosity of a hadron gas was studied up to temperatures of around 160 MeV [16–26], where the hadron gas turns into the quark-gluon plasma in a crossover [27]. Around the transition temperature, results from gluodynamics and QCD on a lattice have provided estimates of η/s [28–31]. In addition to the temperature, the dependence of $\eta(T, \mu_B)$ on the baryon chemical potential was also investigated [19, 21, 32]. It has been observed that the shear viscosity to entropy density ratio reaches a minimum around the phase transition temperatures of everyday substances and several effective models of QCD [23, 25, 33–37], which presents another motivation to study this coefficient. It has been argued that η/s has a minimum at the critical point of a transition between the hadronic matter and the quark-gluon plasma [33], which is currently a subject of intense experimental research.

Hadronic transport approaches aim to describe the effects of hadron rescattering in the last stages of heavy ion collisions. One assumes that soon after hadronization the system is dilute enough that it can be accurately described by a kinetic framework in terms of the Boltzmann equation. Heavy ion collisions at low beam energies, where the production of a quark-gluon plasma is unlikely, can also be appropriately described by such a model. In the latter scenario the medium is dominated by hadrons at all times until the kinetic freeze-out, and the transport approach covers the whole evolution of the system. Several transport codes have been developed to describe experimental observables in heavy ion collisions [38–43].

Our goal is to provide an independent computation of $\eta/s(T, \mu_B)$ in the hadronic phase in the range of $T = 75$ –

175 MeV and $\mu_B = 0-600$ MeV using SMASH (Simulating Many Accelerated Strongly-interacting Hadrons)[44]. The Green-Kubo relation [45, 46] is applied to thermalized hadronic matter in a static box simulating infinite matter. Similar calculations have been performed in [47–52]. The results of existing studies in this range disagree up to a factor of ten and our goal is to understand the discrepancy between them. This question has recently also been addressed in [52], where the authors find a considerable difference between the results from the UrQMD transport code [48] (to which SMASH is closer in conception), and the ones from the B3D transport approach [52, 53]. To get a better understanding of the differences between these approaches, we perform numerical solutions of the Boltzmann equation for simple systems using the Chapman-Enskog expansion including genuine $2 \rightarrow 2$ collisions [25]. The main result of the present study is the explanation of the physical origin of this discrepancy and, more generally, of the differences between transport computations whose interactions are dominated by resonance formation, and those calculations in which binary collisions dominate the dynamics.

In Sec. II we introduce the methodology to compute the shear viscosity of infinite matter. In Sec. II A we review the Green-Kubo technique to extract the value of η for an equilibrated system. Sec. II B presents an overview of the most relevant features SMASH, the transport approach that we used. We describe the process of equilibration and the extraction of thermodynamical quantities of the system in Sec. II C. In Sec. II D we present a calculation in a simple system which allows us to study the systematic effects of the parameters on the calculation. In Sec. III we present our main results for η in different hadronic systems. First, in Sec. III A we study a box with pions interacting via the formation of the ρ resonance and compare it to a semi-analytical solution of the Boltzmann equation of a pure pion gas. Then in Sec. III B we present η/s and $\eta T/w$ (where w is the enthalpy density) for the full hadron gas as a function of the temperature and chemical potential. We compare our results with previous studies in Sec. III C and explain the origin of the main discrepancies between them. Finally we present our conclusions and outlook in Sec. IV.

II. METHODOLOGY

A. Green-Kubo formalism

In this work we employ the Green-Kubo formalism for the shear viscosity calculation. More generally this formalism describes how to relate transport coefficients to dissipative fluxes, which are here understood as fluctuations around a state of equilibrium in a given system [45, 46]. Specifically, assuming a uniform distribution of particles in space, the shear viscosity η is calcu-

lated using

$$\eta = \frac{V}{T} \int_0^\infty dt C^{xy}(t), \quad (1)$$

where V is the volume of the system, T its temperature, t the time and

$$C^{xy}(t) = \langle T^{xy}(0)T^{xy}(t) \rangle_{eq} \quad (2)$$

the auto-correlation function of off-diagonal components of the energy-momentum tensor T^{xy} . In a transport approach such as SMASH, we have access to the full phase space evolution of the system through knowledge of all point-like particles at all times. In a discrete case like this, $C^{xy}(t)$ takes the form

$$C^{xy}(t) = \lim_{N \rightarrow \infty} \frac{1}{N} \sum_{s=0}^N T^{xy}(s\Delta t) T^{xy}(s\Delta t + t), \quad (3)$$

with N being the total number of timesteps taken into consideration (in our calculation $N = 5000$), and Δt being the timestep size. Note that we require the system to remain at thermal and chemical equilibrium. Thus, $t = 0$ is the onset of equilibrium.

The spatially-averaged energy-momentum tensor is defined according to

$$T^{\mu\nu} = \frac{1}{V} \int d^3x \int d^3p \frac{p^\mu p^\nu}{p^0} f(\mathbf{x}, \mathbf{p}), \quad (4)$$

where $f(\mathbf{x}, \mathbf{p})$ is the phase-space density of the particles. Discretized, this yields

$$T^{\mu\nu} = \frac{1}{V} \sum_{i=1}^{N_{part}} \frac{p_i^\mu p_i^\nu}{p_i^0}, \quad (5)$$

where the sum is taken over all particles in the system, N_{part} .

It is generally thought that the auto-correlation function behaves as a decaying exponential [47–50],

$$C^{xy}(t) = C^{xy}(0) e^{-\frac{t}{\tau}}, \quad (6)$$

where we introduce the shear relaxation time τ . Using this ansatz, we find the final expression that will be used to calculate the shear viscosity,

$$\eta = \frac{C^{xy}(0)V\tau}{T}. \quad (7)$$

In a more detailed study of the systematic errors introduced in this method [54], it has been shown that there are significant deviations from the exponential form at high densities ($\mu_B > 600$ MeV, $T > 175$ MeV). Therefore, the results in this work are restricted by this temperature-baryon chemical potential range.

The initial value $C^{xy}(0)$ is also computed analytically after taking the continuum limit of

$$C^{xy}(0) = \langle \sum_i \frac{(p_i^x)^2 (p_i^y)^2}{V^2 (p_i^0)^2} \rangle \rightarrow \int d^3\mathbf{x} d^3p \frac{(p^x)^2 (p^y)^2}{V^2 (p^0)^2} f(p), \quad (8)$$

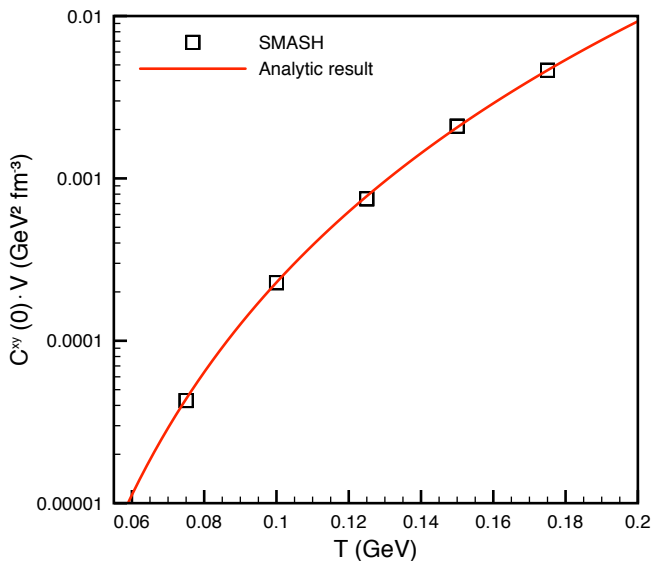


FIG. 1. Volume-independent initial value of the correlation function as a function of temperature, for a system containing one species of particles of mass $m = 138$ MeV.

with $f(p)$ being the Maxwell-Boltzmann distribution function. For a mixture of N (stable) hadrons

$$C^{xy}(0) = \sum_{a=1}^N \frac{g_a z_a}{30\pi^2 V} \int_0^\infty dp \frac{p^6}{m_a^2 + p^2} \exp\left(-\frac{\sqrt{m_a^2 + p^2}}{T}\right), \quad (9)$$

where $z_a = \exp(\mu_a/T)$ is the fugacity of the species a , with a spin-isopin degeneracy factor g_a . Figure 1 shows a comparison of the volume-independent $C^{xy}(0)$ for a single particle system as computed analytically and in SMASH.

One notes that the previous quantity does not depend on any parameter related to the interaction of particles. Hence, all microscopical information about the dynamics of the system (i.e. the cross-sections) is encapsulated within the relaxation time of the correlation function. It can be interpreted as the characteristic time for a fluctuation of T^{xy} to decay, and is expected to be of the order of the mean-free time (unless the cross-section is very forward-peaked).

The calculation in SMASH can in principle be performed by fitting the auto-correlation function to a decaying exponential according to Eq. (6). This yields the parameters $C^{xy}(0)$ and τ . In practice however, problems arise with the upper limit of the sum in Eq. (3). As all simulations run for a finite time, the sum over time intervals is performed over smaller and smaller data sets as the interval grows. Hence, the error on the correlator rapidly increases with growing t and becomes pure noise in the region of high t (see Fig. 2). To cope with this problem we fit only the early part of the auto-correlation function (where the errors are still small) to a decaying

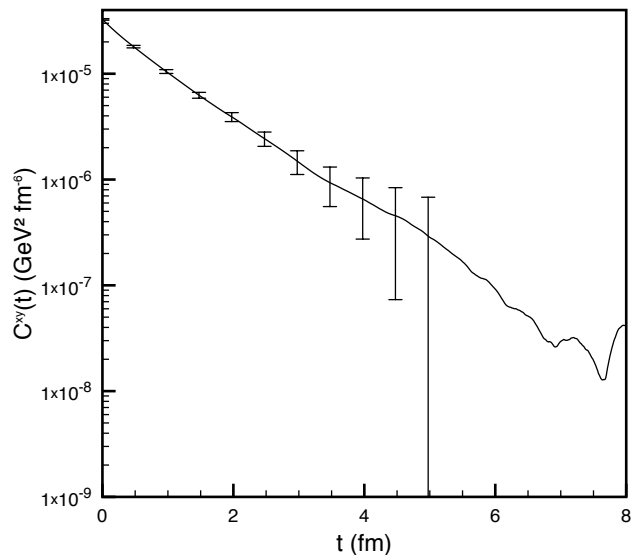


FIG. 2. Typical example of a correlation function, for a massive gas of particles interacting through constant isotropic cross-sections $\sigma = 20$ mb, at temperature $T = 200$ MeV and mass $m = 138$ MeV.

exponential. Yet, such a procedure needs to be handled with caution, as it requires a proper determination of the region to actually fit.

In this work, we use a fit method that relies on calculating the average auto-correlation function from many simulations (typically 1000). The relative error is estimated for each time interval t . As it is known that this error increases as t increases (see Fig. 2), we implement a criterion for the cutoff to happen when the relative error on the average auto-correlation function reaches a given level. By looking at systems of varying complexity we show in Ref. [54] that one should use cutoff values between 4-10%. For all further calculations, a cutoff of 6% was chosen to fit the average correlation function.

B. Hadronic transport: SMASH

SMASH [44] is a recently developed transport approach to describe the hadronic evolution within heavy-ion collisions at different accelerators like the Large Hadron Collider (LHC), the Relativistic Heavy Ion Collider (RHIC) and the SIS-18 at the GSI Helmholtzzentrum für Schwerionenforschung. Effectively, a set of coupled Boltzmann equations [2] for different hadron species,

$$p^\mu \frac{\partial f_i(t, \mathbf{x}, \mathbf{p})}{\partial x^\mu} = C_{coll}[f_i, f_j], \quad (10)$$

where f_i denotes the one-particle distribution function defined in the phase space of the species i , is solved numerically. C_{coll} is the collision integral involving all the

distribution functions of the other species which interact with i .

The particles evolve according to their equations of motion and are allowed to collide. SMASH uses a geometrical collision criterion based on the total cross section (see [44] for details). The degrees of freedom in [44] have been expanded to contain all the well established hadrons listed in [55], except the $\pi_2(1880)$ and $\phi(2170)$ light unflavoured mesons and the $N(1990)$, $N(2600)$ and $\Delta(2420)$ baryons. It is also important to mention that at low energies the interactions among hadrons are assumed to happen via resonance formation (this is supposed to be valid up to \sqrt{s} of several GeV, where resonant structures disappear from hadron-hadron cross sections). Therefore, in the standard application of SMASH, almost all reactions are of the type $2 \rightarrow 1$ and $1 \rightarrow 2$ (with the notable exception of the nucleon-nucleon interaction, where the cross section is introduced as a parametrization of the experimental data).

SMASH is able to mimic an infinite medium by running a “box calculation”, where interactions can be chosen to be either 1) purely elastic with constant $2 \rightarrow 2$ cross sections, 2) based on the previously described resonance model, or 3) a combination of both.

Another issue to consider is the baryon-antibaryon annihilation, which are usually treated by string fragmentation [38–43]. This is however problematic in infinite matter calculations, as detailed balance is not conserved for string fragmentation processes. In other words, while it is possible to annihilate a baryon and an anti-baryon to produce many particles, the reverse process is computationally challenging. One possible solution to this problem is the production of resonances instead of strings in such scatterings. Using an appropriately parametrized cross-section, we rely on the fact that on average, nucleon-antinucleon annihilation produces 5 pions, as it was suggested in [56]. Thus we implement the following reaction:



In SMASH, the ρ resonance decays exclusively to 2π (when neglecting electromagnetic interactions) and the $h_1(1170)$ resonance decays to $\pi\rho$. We then get, after resonance decays, 5 pions from every $\bar{N}N$ interaction. This process is reversible in all steps and we recover detailed balance for nucleon-antinucleon annihilation.

C. Thermodynamic quantities

In complex systems where inelastic collisions are allowed, the chemical composition of the system, its temperature and the chemical potential can change from the initial state if this one is not directly equilibrated. One thus needs a way to calculate the actual values of these thermodynamic quantities in the system after equilibration.

The temperature is obtained by fitting momentum distributions of given particle species:

$$\frac{dN}{dp} \propto p^2 e^{-\frac{\sqrt{p^2+m^2}-\mu}{T}}. \quad (12)$$

Note that the extracted temperatures differ slightly from one species to the next. It is therefore necessary to distinguish between the temperature of a particle species and the temperature of the system. In concrete terms, we will consider the temperature of the system to be the weighted average of the most abundant stable particles in any system (in the case of the full hadron gas described in section III B, this will typically be pions, kaons and nucleons, where their respective multiplicities are taken as weights).

Although there is in theory a different chemical potential for every particle species, we will here only be interested in true conserved quantum numbers; specifically, the baryon chemical potential. It is assumed that the chemical potential of baryons can be approximated by that of nucleons. The latter is obtained by using the ratio of the momentum distributions (Eq. 12) of nucleons to that of anti-nucleons, such that

$$\frac{dN_N/dp}{dN_{\bar{N}}/dp} = \exp\left(\frac{2\mu_B}{T}\right). \quad (13)$$

This ratio is approximately flat in the region which was used for the temperature determination. Its momentum average in this region is calculated and used as a proxy for the baryon chemical potential.

Finally, let us mention that we use the definition of the Gibbs free energy to calculate the entropy density,

$$s = \frac{w - \mu_B n_B}{T} = \frac{\epsilon + P - \mu_B n_B}{T} \quad (14)$$

where we introduce the enthalpy w , energy density ϵ and pressure P . ϵ and P are obtained directly from the diagonal components of the averaged energy-momentum tensor, the temperature T and baryon chemical potential μ_B from Eqs. (12) and (13) and the baryon number density n_B by counting baryons and anti-baryons in a given volume of the system.

As mentioned in section II A, the system is required to be in thermal and chemical equilibrium for the Green-Kubo formalism to be applicable. To ensure that such an equilibrium is reached fast, every particle species density (including resonances) is initialized near the thermal expectation (using Boltzmann statistics), allowing for Poissonian fluctuations, following

$$n_a = \frac{g_a T^3 e^{\mu_a/T}}{2\pi^2} \frac{m_a^2}{T^2} K_2\left(\frac{m_a}{T}\right), \quad (15)$$

where a is a given particle species. Transport model densities in such calculations typically equilibrate to values near the Boltzmann grand canonical expectation. Small

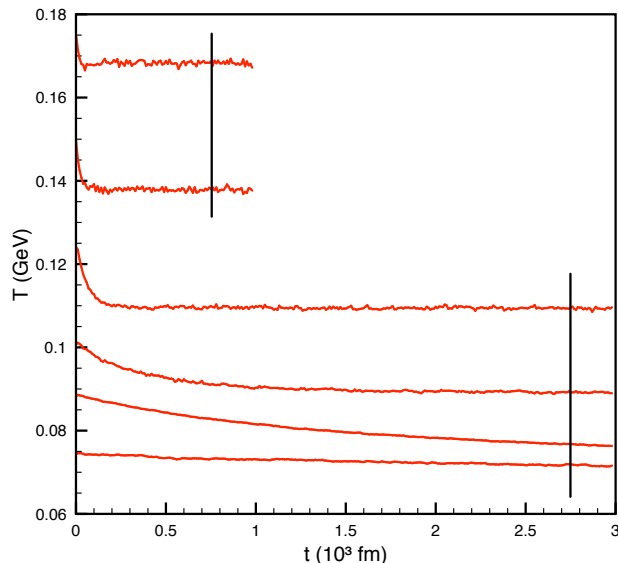


FIG. 3. Temperature evolution of the box over time, for different initial temperatures. The vertical bar shows which part of the evolution is considered as in equilibrium and taken into account in the calculation of the correlation function. Note that the region of thermal equilibrium is in some cases much larger than the considered one.

deviations are expected since the initialization of particle multiplicities does not take into account resonance spectral functions, which leads to slightly different final particle densities. The infinite matter simulation is thus left to equilibrate for an appropriate time, and the viscosity calculation proceeds after both chemical and thermal equilibrium have been reached. The chemical equilibrium is checked by verifying that the multiplicities of the individual species in the box saturate to a stable value (see [44] for examples). Similarly, the thermal equilibrium requirement is checked by monitoring the temperature of the box and waiting for it to reach a saturation value. Thermal equilibration takes much longer than chemical equilibration.

Equilibration times depend strongly on the complexity of the content of the box, more degrees of freedom corresponding to longer equilibration times. In the trivial case presented in the next section, only one species of particles is allowed to interact elastically. In this setup, the system is directly initialized into chemical and thermal equilibrium, since no particle number changing processes can occur. For the full hadron gas, the equilibration process however lasts markedly longer, especially at low temperatures (which is expected, as initial density increases fast as a function of temperature, see Eq. (15)). As seen in Fig. 3, thermal equilibration times for such a system usually range from a couple hundred fm at higher temperatures ($T = 150$ MeV and higher) to several thousand fm at lower temperatures ($T = 100$ MeV and lower).

D. Systematics

One of the simplest hadron gas systems that one can think of is composed of one species of particles that only interacts elastically via a constant isotropic cross-section. These systems have been studied extensively and their shear viscosity can be extracted analytically by linearizing the collision term of the Boltzmann equation using the Chapman-Enskog or relaxation time approximations [50]. As such, this system constitutes the perfect playground for a proof of concept. The main goal of this first study is the evaluation of the systematic error of the present calculation by comparing it to a well-known and understood case.

A numerical solution of the Boltzmann equation is obtained following the methodology of [25]. We implement the Chapman-Enskog expansion [2] to the (nonequilibrium) distribution function in the Boltzmann equation (10). This approach, consistent with the hydrodynamic expansion, allows us to linearize the collision operator and simplify the left-hand side of this equation by replacing the distribution function by the local equilibrium distribution. After expanding the deviation from equilibrium in an appropriate polynomial basis, we transform the integral Boltzmann equation into a matrixial equation which is solved order by order in the polynomial expansion. Matching the microscopic expression of the energy momentum tensor (Eq. 4) with the Newton equation (in the local rest frame, $u^\mu = (1, 0, 0, 0)$)

$$T^{xy} = -\eta \left(\frac{\partial u^x(\mathbf{x})}{\partial y} + \frac{\partial u^y(\mathbf{x})}{\partial x} \right), \quad (16)$$

the value of η is extracted due to small deviations from equilibrium.

Fig. 4 shows the result of a comparison between the SMASH infinite matter calculation employing the Green-Kubo formalism to a 15th order Chapman-Enskog calculation [25]. As is readily apparent, the previously described way to fit the Kubo method reproduces analytical calculations very precisely. The top three panels show the dependence of the shear viscosity on the three physical parameters that appear in this calculation, namely the temperature, the constant elastic cross-section and the mass of the particles, all of these being otherwise kept equal. We remind the reader that the kinetic theory estimates of η for a system of ultrarelativistic particles interacting with a constant cross section is $\eta \sim T/\sigma$ [2, 50] and for nonrelativistic particles is $\eta \sim (Tm)^{1/2}/\sigma$ [25]. We observe that the shear viscosity increases with temperature and mass, and decreases with cross-section. This behavior is expected, since the relaxation time to equilibrium decreases as the cross section and thus the number of collisions increases. The dependence on the cross section is very well approximated by $1/\sigma$, while the precise scaling with T and m follows an intermediate behavior between the nonrelativistic and ultrarelativistic cases.

The three bottom panels of Fig. 4 refer to the method's dependence on more technical parameters. The one on

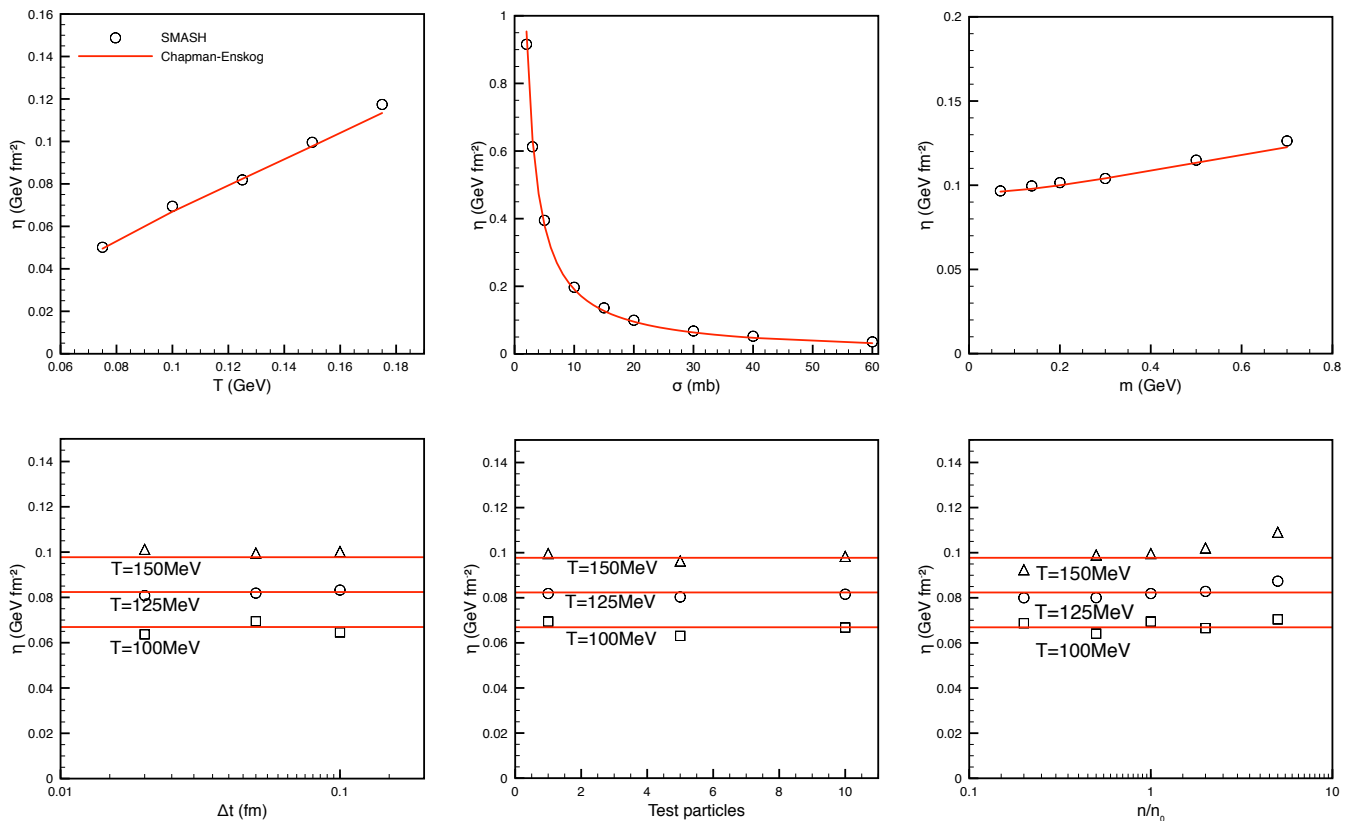


FIG. 4. Single-species gas systematics. Viscosity of a massive gas interacting through constant elastic cross-section, as computed in SMASH (symbols) and a Chapman-Enskog approach (red lines), plotted versus temperature (top left), cross-section (top middle), mass of the particle (top right), time step size between calculations of T^{xy} (bottom left), number of test particles (bottom middle) and density ratio n/n_0 (bottom right), where n_0 is the particle density at zero chemical potential. When not mentioned directly on the plot or on an axis, $T = 0.15$ GeV, $\sigma = 20$ mb and $m = 0.138$ GeV.

the left shows that, provided the use of a sufficiently small timestep size, the result converges to the analytical value. We find that the range of timestep sizes considered is appropriate; all further calculations use a timestep size of 0.05 fm. The bottom middle plot shows the effect of including test particles. In this case each physical particle is divided into multiple ones while correspondingly scaling down each component's cross-section, thus approaching the continuum limit. Very limited effects are observed. Hence, for simplicity, and since the use of many test particles implies heavy computational costs, all further calculations are made using only one physical particle. Note that this result differs from what is found in the literature [50], where the use of hundreds of test particles is recommended. Since τ is independent from N_{test} in a local collision kernel, it follows that the non-locality of the geometrical collision criterion could explain differences in viscosity from the number of test particles [57]. The apparent discrepancy can be explained by the fact that we use similarly large numbers of box calculations instead of test particles for computational convenience. The last plot, to the bottom right, explores the effect of altering the density of the system. In principle, it is well

known that the shear viscosity is independent of the density [58]. Within our calculation however, it is possible that numerics have an effect on observables in some limits. Yet, as the last panel shows, these effects prove to be negligible in most cases, with the exception of very large densities at higher temperatures. In any case, these non-zero deviations remain small with respect to the value of the analytical calculation.

This first test scenario shows that, as expected, the results of the method are mostly unaffected by the variation of non-physical parameters. Thus it is applicable in a wide range of more complex situations. The maximum deviation from analytical calculations is observed to be less than 8%. Therefore, this value is assigned to be our systematic error in all further calculations.

III. RESULTS

Now that a firm basis for the calculation has been established, we use it in a succession of systems of increasing complexity.

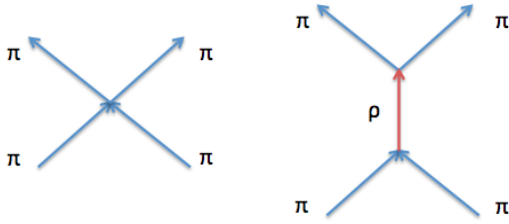


FIG. 5. Sketch of the point-like vs resonant picture of interactions.

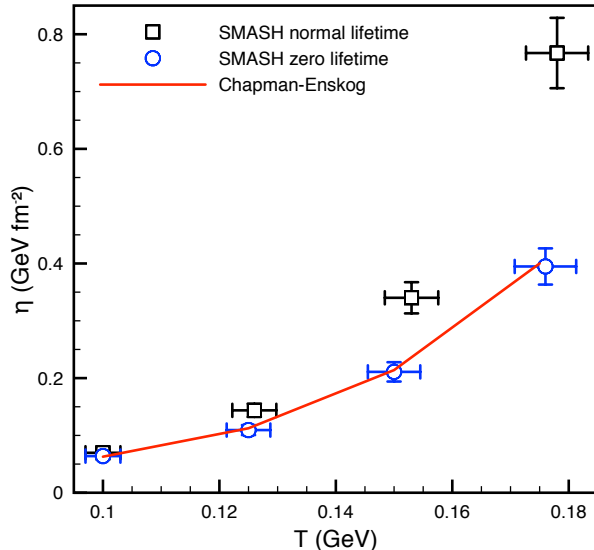


FIG. 6. Shear viscosity vs temperature in a $\pi - \rho$ gas, for different lifetimes and compared to the Chapman-Enskog analytical result.

A. $\pi - \rho$ system

The first system consists of pions interacting through a ρ resonance which is described by a Breit-Wigner mass distribution. In SMASH, the pion pair is produced isotropically.

Analytical calculations of the viscosity of such systems using the Chapman-Enskog formalism exist [16, 17, 25]. These analytical calculations consider a system of pions interacting via a cross-section that reproduces the ρ peak, but the resonance is actually never produced, the outgoing pions being directly created in a point-like interaction. Figure 5 illustrates the schematic difference between the two descriptions; as one can see, the main difference between the two pictures is the fact that in SMASH, the ρ resonance has a finite non-zero lifetime.

For the sake of comparison, several modifications have been made in the approach presented in [25]: 1) only the $(I, J) = (1, 1)$ channel (relevant for the ρ meson) is kept in the $\pi\pi$ scattering, whereas the isoscalar and

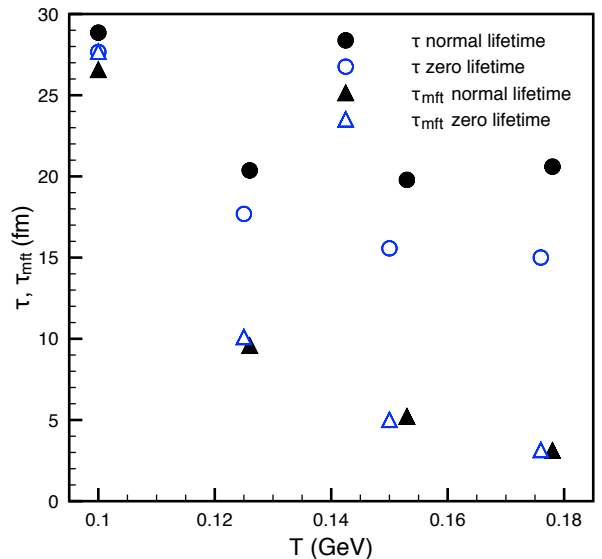


FIG. 7. Relaxation time τ and mean-free time τ_{mft} versus temperature in a $\pi - \rho$ gas, for different lifetimes.

isotensor channels are neglected, 2) in spite of the genuine p -wave scattering in the isovector channel, the differential cross section is tuned to be isotropic for consistency with SMASH¹, and 3) we implement the same scattering amplitude squared from SMASH, but multiplied by a factor 6/9. This is due to the fact that in [25] an average scattering amplitude for all possible 9 initial states $(\pi^\pm, \pi^0) \otimes (\pi^\pm, \pi^0)$ was used, whereas in the simulation we consider only 6 of these combinations (more specifically, scatterings between pions of the same charge are not possible, if including only the ρ meson).

Figure 6 shows the effect of this difference on viscosities, as well as the effect of forcing resonances to decay immediately in our transport model, which effectively sets the lifetime of the ρ resonance to zero and makes interactions point-like. This has the effect of bringing the two results much closer together, to the point where the two calculations are once again in strong agreement.

As shown in Fig. 7, the lowering of the shear viscosity when setting the resonance lifetimes to zero is explained by looking at the relaxation time of the system in both cases. As one can easily see, the relaxation time appears to be increasingly reduced as one goes to higher temperatures; this suggests that the lifetime of resonances can have a large impact on the relaxation time when the lifetime is not negligible with respect to the mean free

¹ The shear viscosity is inversely proportional to the “transport cross section”, $\sigma_{tr}(s) = \int d\Omega \sin^2 \theta d\sigma/d\Omega(s, \theta)$ [50]. For an s -wave isotropic interaction one has $\sigma_{tr} = 2/3\sigma_{tot}$, where σ_{tot} is the total cross section. For a p -wave interaction one has $\sigma_{tr} = 2/5\sigma_{tot}$. Therefore, the shear viscosity of a p -wave interaction is a factor 5/3 larger than the isotropic scattering.

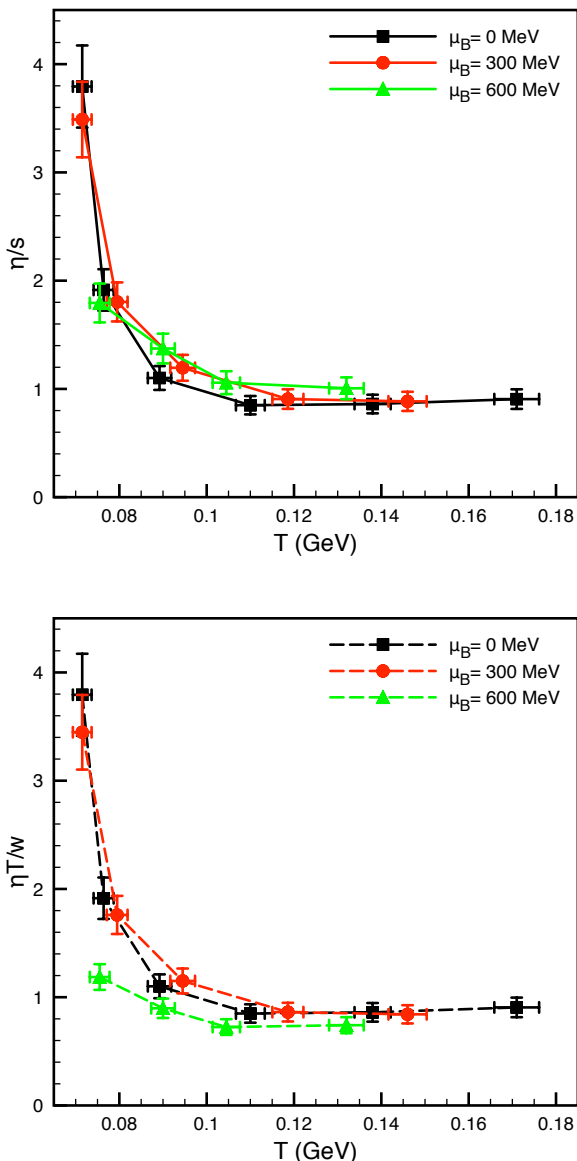


FIG. 8. Shear viscosity to entropy (top) and enthalpy (bottom) density ratios vs temperature, for various baryochemical potentials.

time of the particles in the system. In the latter case notice that τ reaches a plateau at high temperatures. Intuitively, the finite lifetime of the ρ meson delays the momentum transfer and therefore affects the relaxation dynamics. Note as well that the time between pion collisions (or mean free time) τ_{mft} remains unaffected by this change in lifetimes.

B. Full hadron gas

We now proceed to calculate the shear viscosity of a hadron gas as simulated in the SMASH transport ap-

proach. Figure 8 shows both the ratio of shear viscosity to entropy density and the ratio of shear viscosity to enthalpy density. Although the former is used as an input to hydrodynamic simulations [7, 8], it has been argued that the latter provides more insight into the transport properties of dense hadronic matter as this combination appears in the sound attenuation length [59]. Here, both ratios are displayed. If we first look at the zero baryonic chemical potential curves (which are identically the same, as expected), we see that they display a decreasing profile at low temperatures, which corresponds to the expected behavior of a liquid approaching a phase transition [60]. One also notices that the shear viscosity to entropy/enthalpy density ratio reaches a plateau around a temperature of 110 MeV, and stays flat until around 170 MeV, that is, for the whole region around the temperature of 155 MeV at which the phase transition is situated [27]. The ratios start to increase slowly at temperatures higher than 170 MeV, but this is also the temperature above which quark and gluon degrees of freedom are becoming important. In SMASH, the cross-sections via resonance excitation decrease at high energies and therefore our calculation is only meaningful in the hadronic region of the phase diagram.

Moving on to non-zero net baryon chemical potential, it appears that the ratio of shear viscosity to entropy density is relatively independent of μ_B at every plotted temperature, at least until values of the chemical potential of approximately 600-650 MeV. On the contrary, the ratio of shear viscosity to enthalpy density displays a difference when going to higher chemical potential. The difference between the two ratios highlights that the inclusion of the baryonic chemical potential term in the entropy calculation (see Eq. (14)) can at times obscure some trends in the physical picture.

For future reference and to help shed some light on the various features of Fig. 8, we now plot all components individually, namely the shear viscosity, entropy density and enthalpy density (Fig. 9). The top panel of Fig. 9 shows the behavior of shear viscosity, which we find at all values of the chemical potential to be an increasing function of temperature, as expected. Increasing chemical potential also increases shear viscosity at equal temperature for all temperatures, which is also expected.

The bottom panel of Fig. 9 simultaneously shows entropy and enthalpy densities as functions of temperature. Since both of these quantities depend primarily on the energy density of the system, it comes as no surprise that increasing the temperature or baryon chemical potential leads to large increases here as well. Note here that in this plot one sees very well the effect of including the baryonic chemical potential in the entropy calculation, with the difference increasing from zero at $\mu_B = 0$ MeV to differences of 30 at 600 MeV. This can at least partly explain the shape of the corresponding curves in Fig. 8.

In Fig. 10, let us now further decompose the previous results by plotting the shear relaxation time τ , which comes into play in the calculation of the shear viscosity

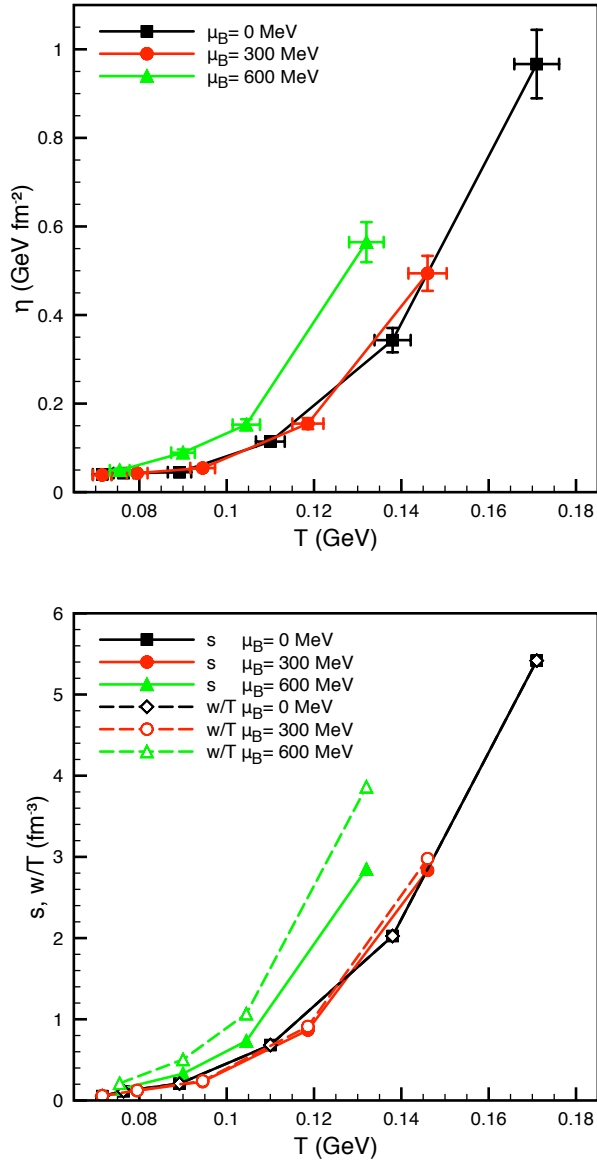


FIG. 9. Shear viscosity (top), entropy and enthalpy densities (bottom) vs temperature, for various baryonic chemical potentials.

(see Eq. (7)). One should first note that the overall profile of these curves is relatively similar to those of Fig. 8. This is expected, since as seen on Fig. 9, $C^{xy}(0)$ rises with the temperature in a way that is approximately matched by the rise in entropy density/enthalpy, so that the final characteristic shape of η/s or $\eta T/w$ is approximately mirroring the shape of the relaxation time.

At higher temperatures, there also appears to be a trend of slightly increasing relaxation time as the baryonic chemical potential increases. Since the composition of the gas is slowly moving towards baryonic matter when increasing μ_B , the baryonic resonances are becoming more prevalent. If we consider that baryons generally

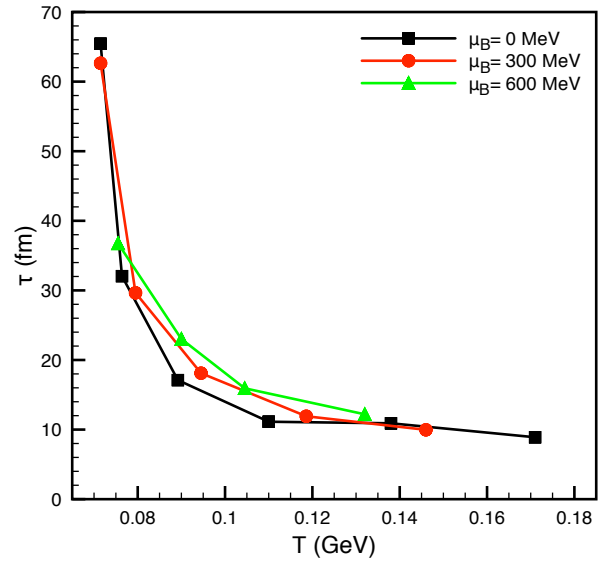


FIG. 10. Shear relaxation time vs temperature, for various baryonic chemical potentials.

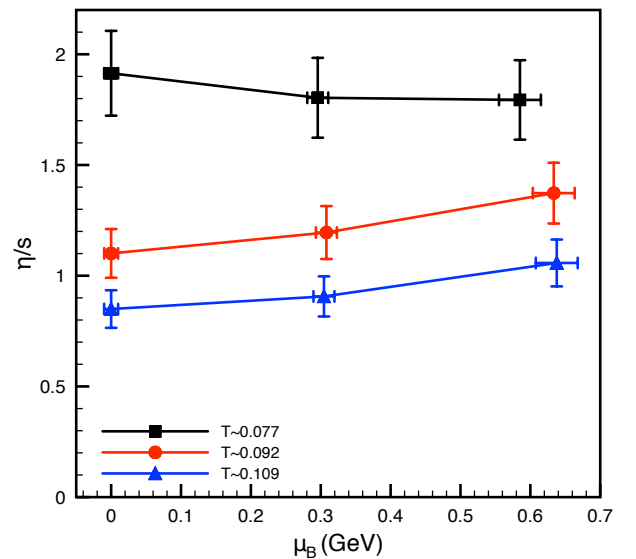


FIG. 11. Shear viscosity to entropy density ratio vs baryonic chemical potential, for various temperatures.

have smaller cross-sections than their mesonic counterparts, this easily explains the observed trend.

Figure 11 shows the same data in a different way: instead of taking temperature profiles at approximately constant baryonic chemical potential, the μ_B dependence of the shear viscosity to enthalpy ratio is investigated at approximately constant temperature. As one can see, we observe for all temperatures a slightly increasing plateau at these values of chemical potential; note that within error bars, this calculation is still consistent with no in-

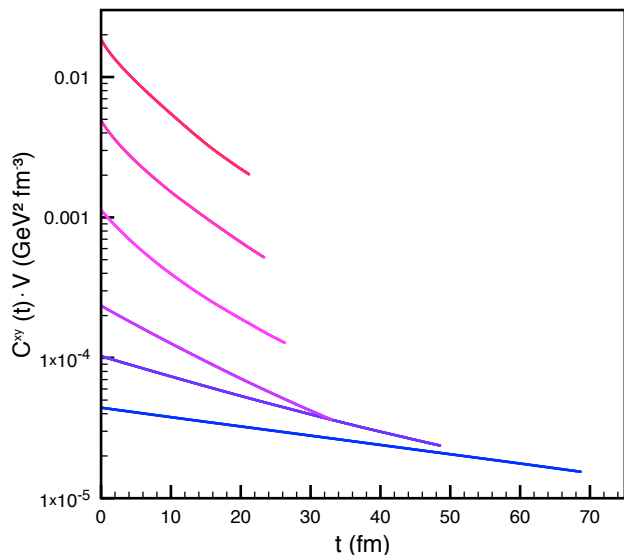


FIG. 12. Typical volume-independent correlation functions for various temperatures at $\mu_B = 0$. From blue to red, or bottom to top, the fitted corresponding temperatures are respectively 71.5, 76.4, 89.2, 110, 138 and 171 MeV. The plotting stops when the relative statistical error reaches 6% in each case, and thus corresponds to the part of the curve which is fitted.

crease at all. The calculated profile of the shear viscosity to entropy ratio at fixed temperature with respect to the baryon chemical potential is actually quite close to what was computed in [21]. Notice that for the current range of temperatures and baryon chemical potentials, it has been checked that the use of Fermi-Dirac instead of Boltzmann statistics has a negligible effect on the observables.

As a reference, we include some typical auto-correlation functions at $\mu_B = 0$ (Fig. 12). As one can readily see, the slope of the function gets steeper with rising temperature; this was directly visible from the previous Fig. 10, where we saw the relaxation time (the inverse of the slope) steadily falling. The slightly non-exponential behavior that one observes is investigated in more detail in [54].

C. Discussion and comparison

In this section, let us first summarize previous calculations of the shear viscosity over entropy density ratio of a hadron gas and then discuss in detail how they compare with our results. As mentioned earlier, the shear viscosity of the hadron gas is an active subject of discussion, and multiple calculations of its value were performed previously, especially for the zero baryon chemical potential case. A comparison of available calculations is presented in Fig. 13. The Demir & Bass [48] calculation uses a similar Green-Kubo formalism, but in the context of the

UrQMD transport code [39]. The Pratt, Baez & Kim [52] curve is computed using the B3D code, but this time by extracting the viscosity from Israel-Stewart equations, while obtaining the necessary other transport coefficients from the Kubo formalism. The Romatschke & Pratt [53] one uses once again the B3D cascade code, with the viscosity η/s being assimilated directly to the response of the energy-momentum tensor to a velocity gradient. The Rougemont et al. curve [32] is computed from a holographic correspondence using the Einstein-Maxwell-Dilaton model. Ozvenchuk et al. [51] use the relaxation time approximation for η applied to the Parton-Hadron-String Dynamics approach [41]. Moroz [26] is an analytical calculation of the hadron gas shear viscosity using the relaxation time approximation and modified UrQMD cross-sections (the EQCS2s set was used). Finally, the χ PT curve uses a Chapman-Enskog expansion to solve the Boltzmann equation relying on the lowest-order scattering amplitude from chiral perturbation theory for the massive pion interaction [25].

Let us now discuss the comparisons for each result starting from the low temperature region. Chiral perturbation theory [61] is the low-energy effective theory of QCD describing the dynamics of the pseudo-Goldstone bosons, associated to the spontaneous symmetry breaking of the chiral symmetry. At lowest order in the chiral expansion, the effective Lagrangian provides the scattering amplitude for the $\pi - \pi$ scattering [62].

The LO χ PT calculation with massive pions provides a model-independent reference value for η/s . However, its validity is restricted to very low temperatures where the system can be approximated to a gas of low-energy pions (up to $T \sim 70$ MeV [21]). At low temperature, SMASH gives values of η/s of the same order of magnitude, but one should not expect a perfect matching to the LO χ PT with our results: in the former, the $I = 1$ channel carries an angular dependent differential cross section (the lowest allowed partial wave is a p -wave) as opposed to isotropic emissions in SMASH (as mentioned earlier, this accounts for differences of the order of up to 5/3 lower viscosity in pion dominated systems). Further differences exist between the transport model and χ PT calculations. As seen on Fig. 14, the dominant $\pi^+\pi^-$ cross section at these low temperatures (which corresponds to the early part of the curve, $\sqrt{s} > 0.7 - 0.8$ GeV) is significantly larger in SMASH (especially when going to higher energies, where χ PT cannot describe any kind of resonant interaction), which also contributes to lower viscosities. The χ PT result additionally contributes to the elastic $\pi^\pm\pi^\pm$ scattering, which is not taken into account in the transport model, although it is expected this will have a more limited effect. Finally, in SMASH the pion scattering occurs by the formation of an intermediate resonance containing the inherent time delay due to its lifetime, which is not implemented in the χ PT calculation. This was mentioned in section III A and will be explained in more detail later, although it should remain much smaller than the other effects at such small temperatures (see

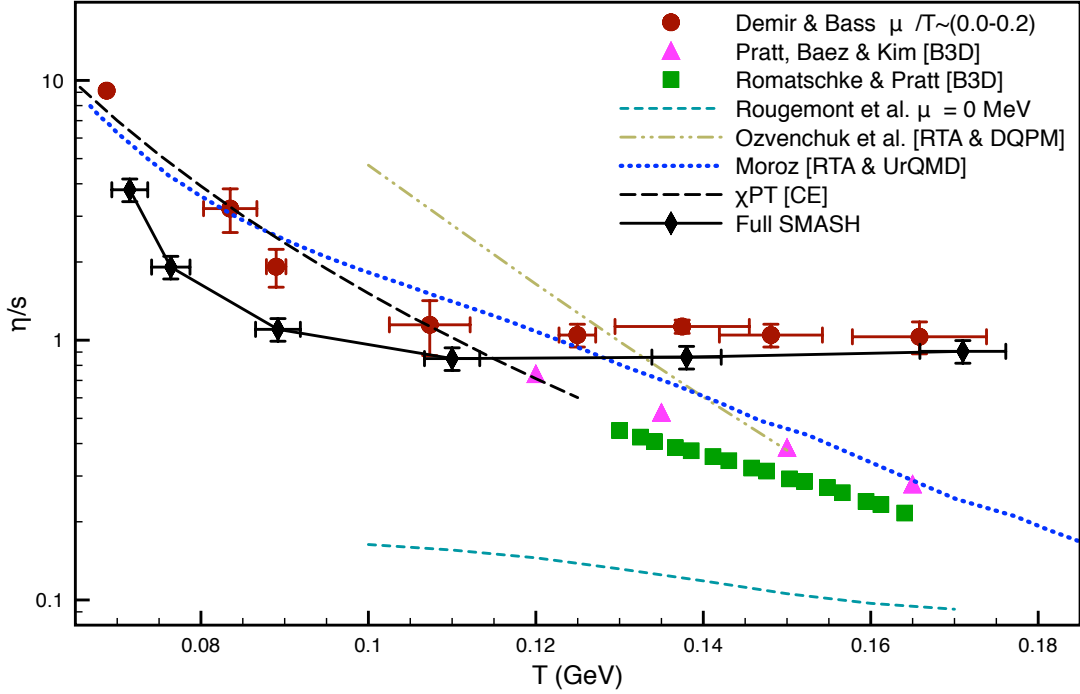


FIG. 13. Comparison of several calculations for the hadron gas η/s at $\mu_B = 0$; see text for details.

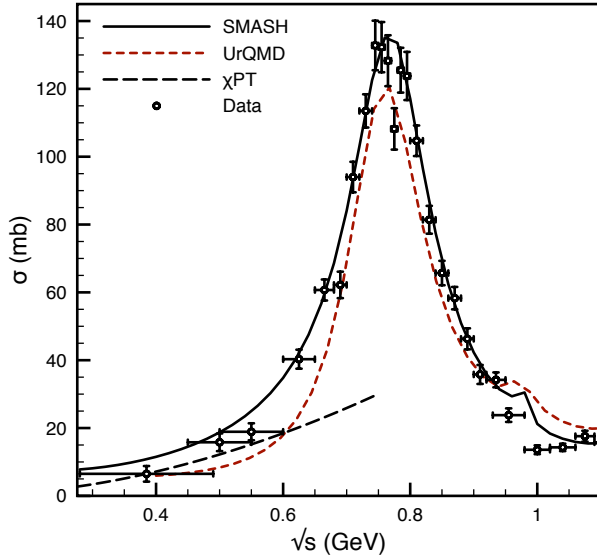


FIG. 14. Total $\pi^+\pi^-$ cross-section in SMASH, UrQMD and LO χ PT, compared to experimental data.

Fig. 6).

Differences between the SMASH and UrQMD description of $\pi\pi$ cross-sections can explain the low temperature discrepancy between our calculation and that of Demir & Bass [48] which used a comparable Green-Kubo

method with this other transport code. Fig. 14 is useful in this regard: although both transport approaches describe reasonably well the experimental data, at low energies SMASH tends to slightly overshoot it while UrQMD slightly undershoots it; this results in a cross-section that is sometimes twice as large in SMASH for this low energy. UrQMD also includes a flat 5mb elastic cross-section for all $\pi\pi$ processes, which could have a slight cancellation effect (although this very small cross-section compared to the much larger inelastic one should not affect viscosity results so much). UrQMD similarly does not account for the p -wave nature of the ρ resonance.

Therefore, an agreement between transport models such as SMASH or the conceptually similar UrQMD and χ PT remains unlikely, and it is then no real surprise that our results remain lower than this calculation at low temperature. As a corollary, although the result from Demir & Bass appears to agree very well with χ PT, this can be accidental to a certain extent.

The Moroz calculation [26] employs an approach to calculate viscosity analytically from the relaxation time approximation in the full hadron gas. The calculation uses a set of improved cross sections from the UrQMD model, including elastic plus quasielastic processes (EQCS2s set). The cross sections are implemented in analytical expressions for the shear viscosity obtained from a Chapman-Enskog expansion of the Boltzmann equations. Although information from resonances is encoded in the cross sections, the collision kernel only contains elastic processes, and no retardation effects from finite lifetimes

are considered. It matches quite well the simpler χ_{PT} expectation at low temperatures; our results however appear to remain consistently larger than this analytical curve for temperatures larger than 130 MeV.

In Ozvenchuk et al. [51] the relaxation time approximation is used to simplify the Boltzmann equation and obtain a simple formula for the shear viscosity. Even when resonance formation is implemented in PHSD simulations, the relaxation time is identified with the mean-free time extracted from collision rates in a box simulation. In this approach, the relaxation time contains no feedback from the resonance lifetimes.

Although exact values differ quite a bit, the general consensus appears to confirm the expectation that the viscosity should generally decrease when approaching a phase transition. That being said, two tendencies are appearing in this plot: some calculations are constantly decreasing for the available data in this range of temperatures, and others appear to saturate at some point and form a plateau at higher temperature; our calculation is among the latter.

Of note, the calculation by Demir & Bass [48] appears to have a similar behavior as ours as temperature increases, the viscosity is also saturating at high temperature. Even though our results are otherwise somewhat smaller, this similarity in the behavior is striking when compared to the other tendency, which predicts a steadier decrease to sometimes much lower values around the critical temperature. One of the common points between UrQMD and SMASH is the treatment of interactions through resonances, which have a non-zero lifetime as illustrated in Fig. 5. In contrast, almost all other calculations use point-like interactions for a great portion of the considered hadronic interactions, if not all. The B3D transport code includes many long-lived resonances, but simultaneously includes an overall constant cross-section of $\sigma = 10$ mb [43], which introduces many point-like interactions, and is thus somewhat hybridized in this regard². Rougemont et al. [32] use the completely different framework of holography, and is therefore excluded from this categorization.

To understand how resonance lifetimes affect the relaxation dynamics, consider a system without physically present resonances. The relaxation time is the characteristic time in which the system approaches equilibrium after a slight departure from it. This time is of microscopic origin, and it is assumed to be of the order of the collision time (or the inverse of the scattering rate). Under a shear perturbation, particles with different momentum will collide redistributing their energy to approach the thermal

distribution. This collision occurs on a time scale of the order of the mean free time, and therefore the relaxation time should be of the same order. If the lifetime of the resonances is finite, but much smaller than the mean free time, then the same picture holds, because the resonance will decay long before the next collision is expected to happen. Therefore, the transport process is unaffected by the generation of a resonance if $\tau_{lifetime} \ll \tau_{mft}$. Again one expects that the relaxation time $\tau \sim \tau_{mft}$. What happens to this picture if resonance lifetime is comparable (or larger) to the mean free time? Then the transport process is blocked until the resonance eventually decays, because it is only at that instant that the momentum exchange is finally performed. The relaxation time is thus now limited by the lifetime of the resonance, becoming independent of the τ_{mft} , as we have checked numerically for the full hadron box (bottom panel of Fig. 15).

This picture breaks down if a sufficient portion of the interactions are point-like. If our explanation is correct, this breakdown in [52] is caused by the large amount of elastic point-like collisions, which happen because of their inclusion of a constant cross-section in B3D. To see if the physical picture that we are depicting holds, let us also apply constant isotropic cross-sections to all interactions in SMASH, so that a significant portion of the collisions will now be point-like. The top panel of Fig. 15 shows the effect of such an adjustment, and we note two differences. The first one is that all points are now at a lower value of shear viscosity, which is explained by the increase in all cross-sections. The second difference is more interesting, and concerns the profile of the curve: rather than saturating at a given value, it now decreases constantly for this range of temperatures, which is what we would expect from a system in which a large part of the interactions is now point-like, so that the relaxation time is not affected by the lifetime of particles anymore.

For further evidence, let us look at the relation between the relaxation time τ and the inverse of the scattering rate, the mean-free time τ_{mft} . In the case of no resonances [52] the relaxation time increases linearly with the collision time, with a proportionality factor of order 1. As seen on the bottom panel of Fig. 15, this expectation is fulfilled in SMASH for low temperatures, when the collision time of particles is much larger than the lifetime of resonances. However, it breaks down at high temperatures, when the collision time decreases to a value where the lifetime of resonances is now large enough to impact the relaxation time of the system, thus forming a plateau around $\tau \sim 10$ fm. When one includes a large number elastic point-like collisions into SMASH, the plateau disappears and we recover a linear dependency of order 1, even at high temperatures. This is once again in line with the expectations of our resonance lifetime hypothesis.

As a final remark, let us now consider the case of non-zero baryon chemical potential, where literature proves to be a lot scarcer, although not inexistent. In this regard we present two comparisons with other calculations (Fig. 16). The first one was made with the similar calcu-

² In principle, UrQMD also includes a point-like elastic cross-section extracted from the Additive Quark Model between all particles. However, on inspection, this elastic cross section turns out to be much smaller than the non-elastic resonance contribution (maximum of 1.35mb in the largest cases, on average almost an order of magnitude smaller). In consequence, only a small number of collisions are point-like in UrQMD.

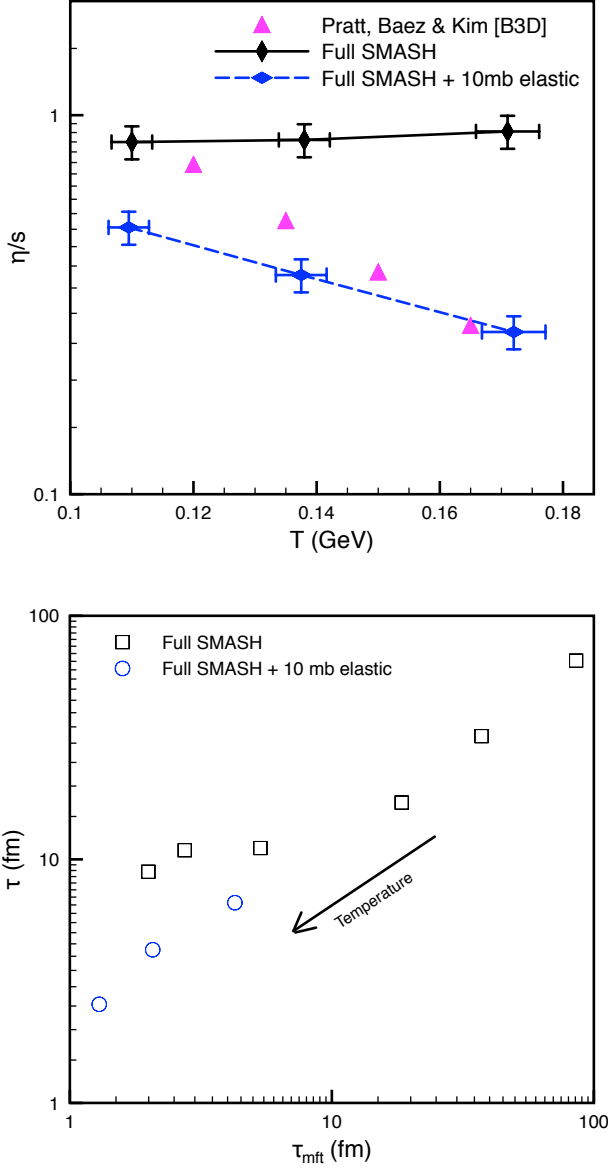


FIG. 15. Effect of adding a constant cross-section to all interactions on the viscosity (top) and on the characteristic times τ and τ_{mft} (bottom).

lation from [48] with UrQMD, and the second one from a holographic approach [32]. In both cases, they observe a difference between the zero and non-zero baryochemical potential results, with the non-zero case yielding a smaller viscosity. In our calculation, both cases are constant within errors. This discrepancy might be explained in the case of Demir & Bass by different methods of calculating the chemical potential term in the entropy (which would also explain why the difference in their curves is growing with temperature); a potential way of seeing whether this is a difference in the actual models would be to compare the shear viscosity to enthalpy ratio instead.

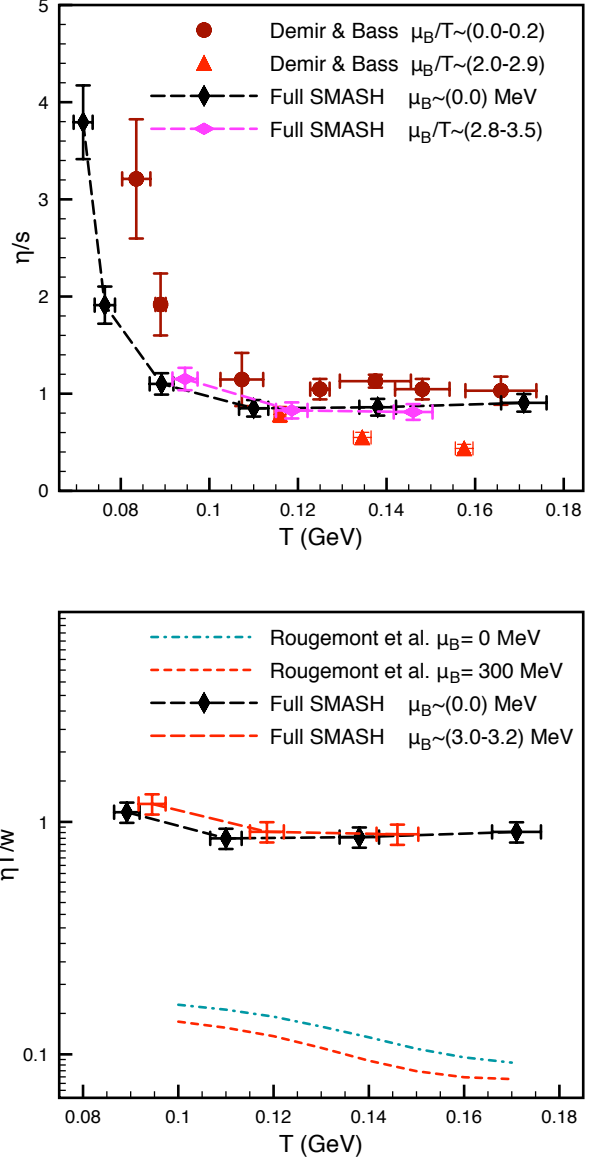


FIG. 16. Non-zero chemical potential comparison with other models of shear viscosity. Comparison is possible with a previous Kubo calculation [48] (top), and a result obtained from holography [32] (bottom)

The approach in [32] is very different in nature, since it goes beyond the quasi-particle picture and assumes strong coupling without confinement. Being close to the holographic result $\eta/s = 1/4\pi$, it is natural that the resulting values of the shear viscosity to entropy ratio are smaller than in our approach. Still, it is interesting to note that the decrease for higher baryon chemical potentials is also observed just for lower values of the chemical potential than in our calculation, where the differences become significant only around $\mu_B = 600$ MeV.

IV. CONCLUSION AND OUTLOOK

After successfully testing the calculation of the viscosity in the recently developed SMASH transport code in the simplest scenario of a single species interacting via constant isotropic cross section, we presented a detailed analysis of the shear viscosity of a hadron gas. The shear viscosity over entropy density coefficient was calculated for hadron matter as a function of temperature and baryon chemical potential, and compared to several results in the literature.

The main conclusion of this study is that the details of the internal dynamics of the system are of crucial importance when comparing transport coefficients in several approaches, as microscopic details can be translated very differently into macroscopic effects. In particular, the different treatment of the hadron-hadron interaction ($2 \rightarrow 2$ elastic collisions versus $2 \rightarrow 1 \rightarrow 2$ quasielastic dispersion) has been seen to have large consequences from the point of view of transport, and the calculation of the transport coefficients.

To turn this around, when more precise values for the temperature dependent viscosity are available from the extraction from experimental data, this could also be used to constrain the treatment of interactions in hadron transport approaches. Along these lines, one can argue that taking into account the medium modifications of the spectral functions of resonances usually results in a broadening and therefore a natural reduction of the lifetime, which counteracts the above described behavior.

In the future, a more rigorous and mathematical analysis of the dependence of the relaxation time on the resonance lifetime and mean free time might provide very useful insights on questions pertaining to their interplay. Second, as previously noted, almost all collisions in transport codes such as SMASH are treated isotropically; as shown previously, the inclusion of more realistic angular distributions can in further investigations have an impact. At temperatures and baryon chemical potentials close to the phase transition, multi-particle interactions will also become relevant and it will be interesting to investigate their influence on the transport coefficients.

ACKNOWLEDGMENTS

We acknowledge Scott Pratt, Steffen Bass, Moritz Greif and Marcus Bleicher for useful discussions and Pierre Moreau for providing the ‘‘Ozvenchuk et al.’’ data in Fig. 13 from [51]. This work was made possible thanks to funding from the Helmholtz Young Investigator Group VH-NG-822 from the Helmholtz Association and GSI, and supported by the Helmholtz International Center for the Facility for Antiproton and Ion Research (HIC for FAIR) within the framework of the Landes-Offensive zur Entwicklung Wissenschaftlich-Oekonomischer Exzellenz (LOEWE) program from the State of Hesse. Computing services were provided by the Center for Scientific Computing (CSC) of the Goethe University Frankfurt.

-
- [1] E. M. Lifschitz and L. P. Pitaevskii, *Course of Theoretical Physics. Vol. 10: Physical Kinetics*, Pergamon Press, (1981)
- [2] S.R. De Groot, W.A. van Leeuwen, and C.G. van Weert, *Relativistic kinetic theory: principles and applications*, North-Holland Publishing Company, the Netherlands, (1980)
- [3] P. F. Kolb, J. Sollfrank and U. W. Heinz, Phys. Rev. C **62**, 054909 (2000) doi:10.1103/PhysRevC.62.054909 [hep-ph/0006129].
- [4] P. Huovinen, P. F. Kolb, U. W. Heinz, P. V. Ruuskanen and S. A. Voloshin, Phys. Lett. B **503**, 58 (2001) doi:10.1016/S0370-2693(01)00219-2 [hep-ph/0101136].
- [5] P. Kovtun, D. T. Son and A. O. Starinets, JHEP **0310**, 064 (2003) doi:10.1088/1126-6708/2003/10/064 [hep-th/0309213].
- [6] P. Kovtun, D. T. Son and A. O. Starinets, Phys. Rev. Lett. **94**, 111601 (2005) doi:10.1103/PhysRevLett.94.111601 [hep-th/0405231].
- [7] P. Romatschke and U. Romatschke, Phys. Rev. Lett. **99**, 172301 (2007) doi:10.1103/PhysRevLett.99.172301 [arXiv:0706.1522 [nucl-th]].
- [8] K. Dusling and D. Teaney, Phys. Rev. C **77**, 034905 (2008) doi:10.1103/PhysRevC.77.034905 [arXiv:0710.5932 [nucl-th]].
- [9] P. Danielewicz and M. Gyulassy, Phys. Rev. D **31**, 53 (1985). doi:10.1103/PhysRevD.31.53
- [10] G. S. Denicol, T. Kodama and T. Koide, J. Phys. G **37**, 094040 (2010) doi:10.1088/0954-3899/37/9/094040 [arXiv:1002.2394 [nucl-th]].
- [11] H. Niemi, G. S. Denicol, P. Huovinen, E. Molnar and D. H. Rischke, Phys. Rev. C **86**, 014909 (2012) doi:10.1103/PhysRevC.86.014909 [arXiv:1203.2452 [nucl-th]].
- [12] H. Song, S. A. Bass and U. Heinz, Phys. Rev. C **83**, 024912 (2011) doi:10.1103/PhysRevC.83.024912 [arXiv:1012.0555 [nucl-th]].
- [13] H. Song, S. A. Bass and U. Heinz, Phys. Rev. C **83**, 054912 (2011) Erratum: [Phys. Rev. C **87**, no. 1, 019902 (2013)] doi:10.1103/PhysRevC.83.054912, 10.1103/PhysRevC.87.019902 [arXiv:1103.2380 [nucl-th]].
- [14] J. E. Bernhard, J. S. Moreland, S. A. Bass, J. Liu and U. Heinz, Phys. Rev. C **94**, no. 2, 024907 (2016) doi:10.1103/PhysRevC.94.024907 [arXiv:1605.03954 [nucl-th]].
- [15] J. Auvinen, I. Karpenko, J. E. Bernhard and S. A. Bass, arXiv:1706.03666 [hep-ph].
- [16] M. Prakash, M. Prakash, R. Venugopalan and G. Welke, Phys. Rept. **227**, 321 (1993). doi:10.1016/0370-1573(93)90092-R
- [17] D. Davesne, Phys. Rev. C **53**, 3069 (1996). doi:10.1103/PhysRevC.53.3069

- [18] A. Dobado and F. J. Llanes-Estrada, Phys. Rev. D **69**, 116004 (2004) doi:10.1103/PhysRevD.69.116004 [hep-ph/0309324].
- [19] S. Muroya and N. Sasaki, Prog. Theor. Phys. **113**, 457 (2005) doi:10.1143/PTP.113.457 [nucl-th/0408055].
- [20] J. W. Chen and E. Nakano, Phys. Lett. B **647**, 371 (2007) doi:10.1016/j.physletb.2007.02.026 [hep-ph/0604138].
- [21] K. Itakura, O. Morimatsu and H. Otomo, Phys. Rev. D **77**, 014014 (2008) doi:10.1103/PhysRevD.77.014014 [arXiv:0711.1034 [hep-ph]].
- [22] M. I. Gorenstein, M. Hauer and O. N. Moroz, Phys. Rev. C **77**, 024911 (2008) doi:10.1103/PhysRevC.77.024911 [arXiv:0708.0137 [nucl-th]].
- [23] A. Dobado, F. J. Llanes-Estrada and J. M. Torres-Rincon, Phys. Rev. D **79**, 014002 (2009) doi:10.1103/PhysRevD.79.014002 [arXiv:0803.3275 [hep-ph]].
- [24] D. Fernandez-Fraile and A. Gomez Nicola, Theory, Eur. Phys. J. C **62**, 37 (2009) doi:10.1140/epjc/s10052-009-0935-0 [arXiv:0902.4829 [hep-ph]].
- [25] J. M. Torres-Rincon, *Hadronic Transport Coefficients from Effective Field Theories*, Springer International Publishing, Switzerland, (2014) doi:10.1007/978-3-319-00425-9 arXiv:1205.0782 [hep-ph].
- [26] O. N. Moroz, arXiv:1301.6670 [hep-ph].
- [27] Y. Aoki, G. Endrodi, Z. Fodor, S. D. Katz and K. K. Szabo, Nature **443**, 675 (2006) doi:10.1038/nature05120 [hep-lat/0611014].
- [28] H. B. Meyer, Phys. Rev. D **76**, 101701 (2007) doi:10.1103/PhysRevD.76.101701 [arXiv:0704.1801 [hep-lat]].
- [29] H. B. Meyer, Nucl. Phys. A **830**, 641C (2009) doi:10.1016/j.nuclphysa.2009.09.053 [arXiv:0907.4095 [hep-lat]].
- [30] S. W. Mages, S. Borsnyi, Z. Fodor, A. Schfer and K. Szab, PoS LATTICE **2014**, 232 (2015).
- [31] N. Astrakhantsev, V. Braguta and A. Kotov, JHEP **1704**, 101 (2017) doi:10.1007/JHEP04(2017)101 [arXiv:1701.02266 [hep-lat]].
- [32] R. Rougemont, R. Critelli, J. Noronha-Hostler, J. Noronha and C. Ratti, arXiv:1704.05558 [hep-ph].
- [33] L. P. Csernai, J. I. Kapusta and L. D. McLerran, Phys. Rev. Lett. **97**, 152303 (2006) doi:10.1103/PhysRevLett.97.152303 [nucl-th/0604032].
- [34] J. W. Chen, M. Huang, Y. H. Li, E. Nakano and D. L. Yang, Phys. Lett. B **670**, 18 (2008) doi:10.1016/j.physletb.2008.10.024 [arXiv:0709.3434 [hep-ph]].
- [35] C. Sasaki and K. Redlich, Nucl. Phys. A **832**, 62 (2010) doi:10.1016/j.nuclphysa.2009.11.005 [arXiv:0811.4708 [hep-ph]].
- [36] A. Dobado, F. J. Llanes-Estrada and J. M. Torres-Rincon, Phys. Rev. D **80**, 114015 (2009) doi:10.1103/PhysRevD.80.114015 [arXiv:0907.5483 [hep-ph]].
- [37] M. Bluhm, B. Kampfer and K. Redlich, Phys. Rev. C **84**, 025201 (2011) doi:10.1103/PhysRevC.84.025201 [arXiv:1011.5634 [hep-ph]].
- [38] W. Ehehalt and W. Cassing, Nucl. Phys. A **602**, 449 (1996). doi:10.1016/0375-9474(96)00097-8
- [39] S. A. Bass *et al.*, Prog. Part. Nucl. Phys. **41**, 255 (1998) [Prog. Part. Nucl. Phys. **41**, 225 (1998)] doi:10.1016/S0146-6410(98)00058-1 [nucl-th/9803035].
- [40] Y. Nara, N. Otuka, A. Ohnishi, K. Niita and S. Chiba, Phys. Rev. C **61**, 024901 (2000) doi:10.1103/PhysRevC.61.024901 [nucl-th/9904059].
- [41] W. Cassing and E. L. Bratkovskaya, Nucl. Phys. A **831**, 215 (2009) doi:10.1016/j.nuclphysa.2009.09.007 [arXiv:0907.5331 [nucl-th]].
- [42] O. Buss *et al.*, Phys. Rept. **512**, 1 (2012) doi:10.1016/j.physrep.2011.12.001 [arXiv:1106.1344 [hep-ph]].
- [43] J. Novak, K. Novak, S. Pratt, J. Vredevogd, C. Coleman-Smith and R. Wolpert, Phys. Rev. C **89**, no. 3, 034917 (2014) doi:10.1103/PhysRevC.89.034917 [arXiv:1303.5769 [nucl-th]].
- [44] J. Weil *et al.*, Phys. Rev. C **94**, no. 5, 054905 (2016) doi:10.1103/PhysRevC.94.054905 [arXiv:1606.06642 [nucl-th]].
- [45] M. Toda, R. Kubo and N. Saito, *Statistical Physics I*, Springer-Verlag, Berlin, (1992)
- [46] R. Zubarev, O. Morozov, *Statistical Mechanics of Nonequilibrium Processes. Vol. 2: Relaxation and Hydrodynamics Processes*, Akademie Verlag GmbH, (1996)
- [47] A. Muronga, Phys. Rev. C **69**, 044901 (2004) doi:10.1103/PhysRevC.69.044901 [nucl-th/0309056].
- [48] N. Demir and S. A. Bass, Phys. Rev. Lett. **102**, 172302 (2009) doi:10.1103/PhysRevLett.102.172302 [arXiv:0812.2422 [nucl-th]].
- [49] C. Wesp, A. El, F. Reining, Z. Xu, I. Bouras and C. Greiner, Phys. Rev. C **84**, 054911 (2011) doi:10.1103/PhysRevC.84.054911 [arXiv:1106.4306 [hep-ph]].
- [50] S. Plumari, A. Puglisi, F. Scardina and V. Greco, Phys. Rev. C **86**, 054902 (2012) doi:10.1103/PhysRevC.86.054902 [arXiv:1208.0481 [nucl-th]].
- [51] V. Ozvenchuk, O. Linnyk, M. I. Gorenstein, E. L. Bratkovskaya and W. Cassing, Phys. Rev. C **87**, no. 6, 064903 (2013) doi:10.1103/PhysRevC.87.064903 [arXiv:1212.5393 [hep-ph]].
- [52] S. Pratt, A. Baez and J. Kim, Phys. Rev. C **95**, no. 2, 024901 (2017) doi:10.1103/PhysRevC.95.024901 [arXiv:1610.07239 [nucl-th]].
- [53] P. Romatschke and S. Pratt, arXiv:1409.0010 [nucl-th].
- [54] J.-B. Rose, J. M. Torres-Rincon, D. Oliinychenko, A. Schäfer and H. Petersen, arXiv:1709.00369 [nucl-th].
- [55] C. Patrignani *et al.* [Particle Data Group], Chin. Phys. C **40**, no. 10, 100001 (2016). doi:10.1088/1674-1137/40/10/100001
- [56] N. S. Demir, *Extraction of Hot QCD Matter Transport Coefficients Utilizing Microscopic Transport Theory*, Ph.D. Dissertation, Duke University (2010)
- [57] S. Cheng, S. Pratt, P. Csizmadia, Y. Nara, D. Molnar, M. Gyulassy, S. E. Vance and B. Zhang, Phys. Rev. C **65**, 024901 (2002) doi:10.1103/PhysRevC.65.024901 [nucl-th/0107001].
- [58] J. C. Maxwell, Phil. Trans. R. Soc. Lond., 156, 249268, (1866) doi:10.1098/rstl.1866.0013
- [59] D. Teaney, Phys. Rev. C **68**, 034913 (2003) doi:10.1103/PhysRevC.68.034913 [nucl-th/0301099].
- [60] D. J. Evans and G. P. Morriss, *Statistical Mechanics of Nonequilibrium Liquids*, Academic, London, (1990)
- [61] J. Gasser and H. Leutwyler, Annals Phys. **158**, 142 (1984). doi:10.1016/0003-4916(84)90242-2
- [62] S. Scherer, Adv. Nucl. Phys. **27**, 277 (2003) [hep-ph/0210398].